

The impact of (n,γ) cross section uncertainties of unstable isotopes near $N = 50$ on nucleosynthesis models of the i process in He-shell flash white dwarfs

Pavel Denissenkov^{1,2,10}, Christian Ritter^{1,2,10}, Marco Pignatari^{3,4,10}, Samuel Jones^{9,10}, Stylianos Nikas^{2,6}, Georgios Perdikakis^{2,5,6}, Hendrik Schatz^{2,5,7,10}, Artemis Spyrou^{2,5,7}, Kathrin Göbel^{8,10}, Benedikt Thomas^{8,10} and Falk Herwig^{1,2,10}

¹Department of Physics & Astronomy, University of Victoria, P.O. Box 1700, STN CSC, Victoria, B.C., V8W 2Y2, Canada

²Joint Institute for Nuclear Astrophysics, Center for the Evolution of the Elements, Michigan State University, 640 South Shaw Lane, East Lansing, MI 48824, USA

³E.A. Milne Centre for Astrophysics, Department of Physics & Mathematics, University of Hull, HU6 7RX, United Kingdom

⁴Konkoly Observatory, Research Centre for Astronomy and Earth Sciences, Hungarian Academy of Sciences, Budapest, Konkoly Thege Miklós út 15-17, 1121 Budapest, Hungary

⁵National Superconducting Cyclotron Laboratory, Michigan State University, East Lansing, MI 48824, USA

⁶Department of Physics, Central Michigan University, Mt. Pleasant, Michigan 48859, USA

⁷Department of Physics & Astronomy, Michigan State University, East Lansing, Michigan 48824, USA

⁸Institute for Applied Physics, Goethe University Frankfurt, Max-von-Laue-Str. 1, 60438 Frankfurt am Main, Germany

⁹Heidelberg Institute for Theoretical Studies, Schloss-Wolfsbrunnengasse 35, 69118 Heidelberg, Germany

¹⁰NuGrid Collaboration, **URL:** <http://www.nugridstars.org>

E-mail: nugrid@lists.uvic.ca

Abstract. The first peak s-process elements Rb, Sr, Y and Zr in the post-AGB star Sakurai's object (V4334 Sagittarii) are the result of i-process nucleosynthesis in a post-AGB very-late thermal pulse event. The remaining discrepancies between the observed and predicted elemental abundance distributions may be due to uncertain nuclear physics data used in the simulations. We identify the unstable isotopes of Br, Kr, Rb, Sr, Y and Zr whose (n,γ) cross section uncertainties will affect simulation predictions. We show that simple, but fast, one-zone simulations can be used instead of more realistic multi-zone stellar simulations for extensive nuclear sensitivity and uncertainty studies, provided that the one-zone setup is first calibrated using the multi-zone simulations. We find that among the 52 unstable isotopes selected for our analysis only uncertainties in the (n,γ) cross sections of ^{85}Br , ^{88}Kr and ^{89}Kr have significant effects on the predicted abundances of Rb, Sr, Y and Zr. A further analysis, that used multi-zone simulations, has shown that the uncertainty in the (n,γ) cross section of

^{89}Rb may also be important in this case. Our findings apply more generally to any i -process site with similar neutron exposure, such as possibly rapidly accreting white dwarfs.

PACS numbers: 26.20.Fj, 25.40.Lw

Keywords: nuclear reactions, nucleosynthesis, stars: abundances, stars: AGB and post-AGB

Submitted to: *J. Phys. G: Nucl. Part. Phys.*

1. Introduction

Most of the Solar System chemical elements heavier than iron were produced in the slow (s) and rapid (r) processes of neutron capture in previous generations of stars and stellar explosions (Käppeler et al., 2011; Thielemann et al., 2011). In the 1970s, Cowan and Rose (1977) proposed that, under certain physical conditions, an *i* process with a neutron density $N_n \sim 10^{15} \text{ cm}^{-3}$ intermediate between those typical for the s ($N_n \leq 10^{11} \text{ cm}^{-3}$) and r ($N_n \geq 10^{20} \text{ cm}^{-3}$) processes might be triggered in stars. Like for the main s process, neutrons for the *i* process are released in the reaction $^{13}\text{C}(\alpha, n)^{16}\text{O}$. The higher neutron density in the *i* process is achieved at typical He-burning temperatures $T \sim 2 - 3 \times 10^8 \text{ K}$ thanks to replenishment of ^{13}C from the reaction $^{12}\text{C}(\text{p}, \gamma)^{13}\text{N}$ followed by the decay $^{13}\text{N}(\text{e}^+ \nu)^{13}\text{C}$. A combination of the He and H burning reactions in one process is possible in a He-flash convective zone, where there is a plenty of He and ^{12}C , provided that a small amount of H is ingested into it when the upper convective boundary reaches the H-rich envelope layer. In this situation, the reactions $^{12}\text{C}(\text{p}, \gamma)^{13}\text{N}$ and $^{13}\text{C}(\alpha, n)^{16}\text{O}$ are spatially separated, each taking place at its own favourable conditions, and ^{13}N with a half life of 9.96 min decays into ^{13}C , while being carried down by convection with a comparable turnover timescale of $\sim 15 \text{ min}$. Whether or not ^{13}N will capture another proton depends primarily on the H to ^{12}C abundance ratio.

It was not until the late 1990s that the first strong evidence of the *i* process in stars was detected. Asplund et al. (1999) investigated the evolution of the surface abundances in the post-AGB star Sakurai's object (V4334 Sagittarii), that was experiencing a real-time nova-like transient outbreak. It was soon interpreted as a very late thermal pulse (Herwig, 2001a, VLTP) of the He-shell on the white-dwarf cooling sequence (Herwig, 2001b; Miller Bertolami et al., 2006). The observations covered a time interval of about six months, during which the abundances of light s-process elements, such as Rb, Sr, Y and Zr enhanced by approximately 2 dex and even showed a further increase over the observational period. These abundance signatures cannot normally arise during the preceding Asymptotic Giant Branch (AGB) evolution, and therefore provide the evidence of active stellar nucleosynthesis during some point of the He-shell flash. According to the stellar evolution models, there is a lag time of a few years (corresponding to the thermal time scale of the remaining thin envelope layer) between the actual nucleosynthesis flash event and the abundance observations. Therefore the observed abundance gradients over the six-month observational period probably signal mixing events rather than ongoing nucleosynthesis.

Herwig et al. (2011) suggested that both the observed changes of the surface chemical composition of Sakurai's object and its light curve resulted from a He-shell flash that led to the physical conditions required for the *i* process, in particular, the vigorous convection that entrains H from a thin H-rich envelope. Within the one-dimensional modelling approach adopted by Herwig et al. (2011) it was also necessary to assume that the He convective zone in Sakurai's object split into two separate convective zones, the upper zone being driven by burning of the entrained H, and that the split occurred

at a later time than predicted by mixing-length theory in the stellar evolution models. Recent three-dimensional simulations of H ingestion in Sakurai's object have revealed global horizontal oscillations of material near the top of the He convective zone caused by the violent burning of ingested H that resulted in a transient split of the convective zone (Herwig et al., 2014), but this is not the split that quenches the *i* process, because not enough H has been burned at that time. Further investigations of the three-dimensional hydrodynamic nature of the convective-reactive He-shell flash with H ingestion in post-AGB stars are needed, due to the complexity of the analysis and present controversial theoretical results (Herwig et al., 2011; Stancliffe et al., 2011; Herwig et al., 2014).

Recently, a number of new abundance measurements with peculiarities potentially due to the *i* process have been made for different types of stars. This may indicate that *i*-process activation is not limited to post-AGB stars. Among these measurements are the peculiar abundances of elements heavier than Fe in some of the carbon enhanced metal poor stars seemingly enhanced in *r*- and *s*-process elements (CEMP-*r/s*) (Beers and Christlieb, 2005; Masseron et al., 2010; Lugaro et al., 2012; Bisterzo et al., 2012). These are stars, in which the observed abundance pattern neither resembles an *r*-process nor an *s*-process, and has traditionally been attributed to a superposition of *s*- and *r*-process contributions. For some of these CEMP-*r/s* stars, e.g. CS 31062-050, the observed elemental abundances are consistent with predictions from *i*-process models, while the traditional scenario of a superposition of yields from the *s* and *r* processes shows discrepancies (Dardelet et al., 2014). The striking result of Dardelet et al. (2014) was that the observed abundances of several CEMP-*r/s* stars could be reproduced using simple one-zone simulations, with constant temperature and density. A reasonable fit was obtained with the typical *i*-process neutron number density $N_n \sim 10^{15} \text{ cm}^{-3}$ and neutron exposure of $\tau \sim 10 - 50 \text{ mbarn}^{-1}$. These results have been recently confirmed by Hampel et al. (2016).

A possible *i*-process contribution has also been invoked in young open clusters, to explain the largest $[\text{Ba}/\text{La}]_{\ddagger}$ ratios that are neither compatible with the *s* process nor with a combination of *s* and *r* processes (Mishenina et al., 2015). Anomalous isotopic abundances possibly originating from an *i* process were also found in some of presolar graphite grains (Jadhav et al., 2013), presolar SiC grains of type AB (Fujiya et al., 2013) and of type mainstream (Liu et al., 2014). And finally, Roederer et al. (2016) proposed that the unusual $[\text{As}/\text{Ge}]$ ratio ($+0.99 \pm 0.23$) and the enhanced $[\text{Mo}/\text{Fe}]$ and $[\text{Ru}/\text{Fe}]$ ratios in the metal-poor star HD 94028 are the signatures of an *i*-process contribution with an even lower neutron exposure compared to the case of Sakurai's object.

With such a diverse set of observational indications it is conceivable that the *i* process is activated in several additional types of stars at various evolutionary stages. Stellar evolution models that include a possible *i*-process nucleosynthesis site target the He-core flash in low-mass stars (Campbell et al., 2010), the He-shell flash in a metal-poor AGB star (Fujimoto et al., 2000; Herwig, 2003; Iwamoto et al., 2004) or super-AGB

\ddagger We use the standard spectroscopic notation $[\text{A}/\text{B}] = \log_{10}(N(\text{A})/N(\text{B})) - \log_{10}(N_{\odot}(\text{A})/N_{\odot}(\text{B}))$, where $N(\text{X})$ and $N_{\odot}(\text{X})$ are abundances of an element X in a star and the Sun.

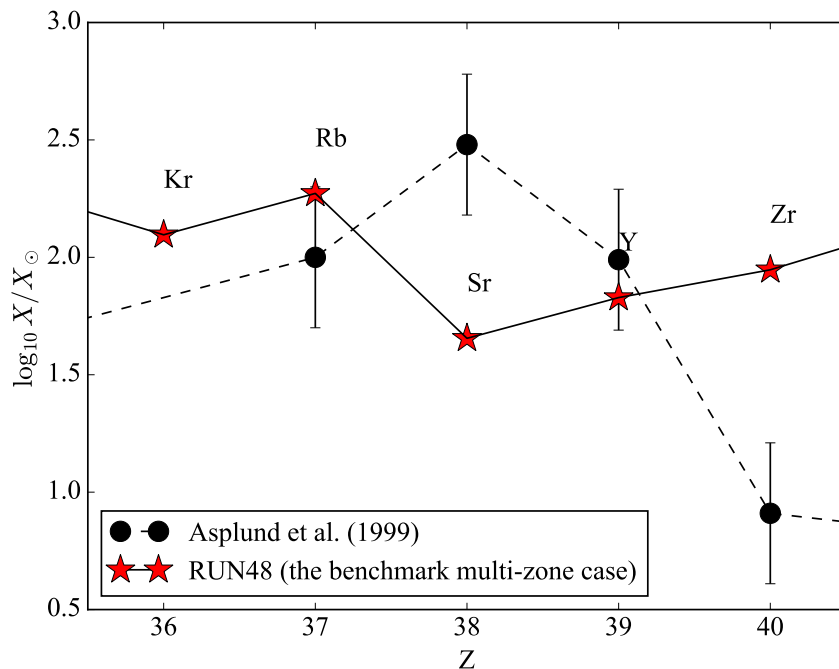


Figure 1. The observed (black circles with errorbars from Asplund et al. (1999)) and predicted (red stars for the benchmark RUN48 model from Herwig et al. (2011)) solar-scaled abundances of Rb, Sr, Y and Zr for Sakurai’s object. The predicted abundances are from multi-zone simulations with a delayed split of the He convective zone. There are quite large discrepancies between the observed and predicted abundances of Sr and Zr that can potentially be caused by stellar model inadequacies, reaction rate uncertainties or observational errors.

stars (Jones et al., 2016).

When studying a specific stellar nucleosynthesis site, e.g. Sakurai’s object, and comparing predicted and observed element abundances, it is important to understand the main reasons behind a successful reproduction of the observations, and behind more disappointing results. Stellar model inadequacies, nuclear physics uncertainties and observational errors can potentially all play a role. The simplest way to analyze them is to disentangle each relative contribution step by step. An example of such disentanglement was the assumption that one-dimensional stellar evolution models were wrong in their prediction of the too early split of the He convective zone in Sakurai’s object that resulted in much lower predicted abundances of Rb, Sr, Y and Zr than the observed ones. As we have already mentioned, the hypothesis of the delayed split proposed by Herwig et al. (2011) within the framework of one-dimensional models allowed them to reproduce the global abundance distribution in Sakurai’s object.

However, a closer look at the predicted and observed abundances of Rb, Sr, Y and Zr in Sakurai’s object in figure 1 reveals that there are still quite large discrepancies for Sr and Zr, especially considering the ratios of the predicted and observed abundance distributions for the first peak s-process elements Rb, Sr, Y and Zr (solid and dashed curves in figure 1).

Sakurai’s object is a unique laboratory to study the *i* process in stars and the details about the physics required to correctly simulate H ingestion. There are no other known nucleosynthesis models that can explain the observations in Sakurai’s object, other than the *i* process. Therefore, these discrepancies become a goldmine for theory. One obvious source of these discrepancies is the three-dimensional nature of the convective-reactive H-ingestion flash as shown by Herwig et al. (2014). Another possible source is the underlying stellar model parameters. For example, Miller Bertolami and Althaus (2007) suggested that Sakurai’s object may have a slightly smaller mass compared to $0.604 M_{\odot}$ assumed in our model. This could have an impact on the details of the mixing events in the He-shell flash. Finally, since the nucleosynthetic pathway of the *i* process involves almost exclusively unstable species it is an obvious concern that nuclear data uncertainties play a major role in this case.

The main goals of this work are therefore

- (i) to determine if and to what extent the discrepancies between observations and model predictions are affected by uncertainties in the (n,γ) cross sections of unstable isotopes relevant to the *i*-process nucleosynthesis of Rb, Sr, Y and Zr in Sakurai’s object;
- (ii) to test if and under what circumstances the one-zone nucleosynthesis simulations can be used in lieu of more time-consuming multi-zone simulations as an analysis tool for reaction rates in nuclear uncertainty and sensitivity studies.

The paper is organized as follows. In section 2, we estimate total variation factors for the (n,γ) cross sections allowed by the nuclear physics for the unstable isotopes relevant to the problem of *i*-process nucleosynthesis of Rb, Sr, Y and Zr in Sakurai’s object. In section 3, we describe the methods and models used in our nucleosynthesis simulations. In section 4, the main results of our uncertainty study are presented. A summary and conclusions are given in section 5.

2. Variation factors for the (n,γ) cross sections relevant to the *i*-process nucleosynthesis of Rb, Sr, Y and Zr in Sakurai’s object

The *i*-process scenario is able to explain the efficient production of the elements at the Sr peak without producing Ba and La, as observed in Sakurai’s object (Asplund et al., 1999). However, the agreement of *i*-process model predictions and observations for Sakurai’s object is still not perfect, and several discrepancies exist, e.g. the predicted $[\text{Rb}/\text{Sr}]$ and $[\text{Zr}/\text{Y}]$ ratios differ from the observed ones at least by 0.3 dex, even if we take the observational errors into account (figure 1). In order to draw any final conclusions about the origin of these unique abundance patterns, and the possible conditions at an *i*-process site, it is therefore critical to understand the origin of these discrepancies. This first requires an analysis of the associated nuclear physics uncertainties. The *i*-process nucleosynthesis calculations rely on neutron capture rates and beta decay rates along the *i*-process path, which proceeds from two to five neutrons away from the valley

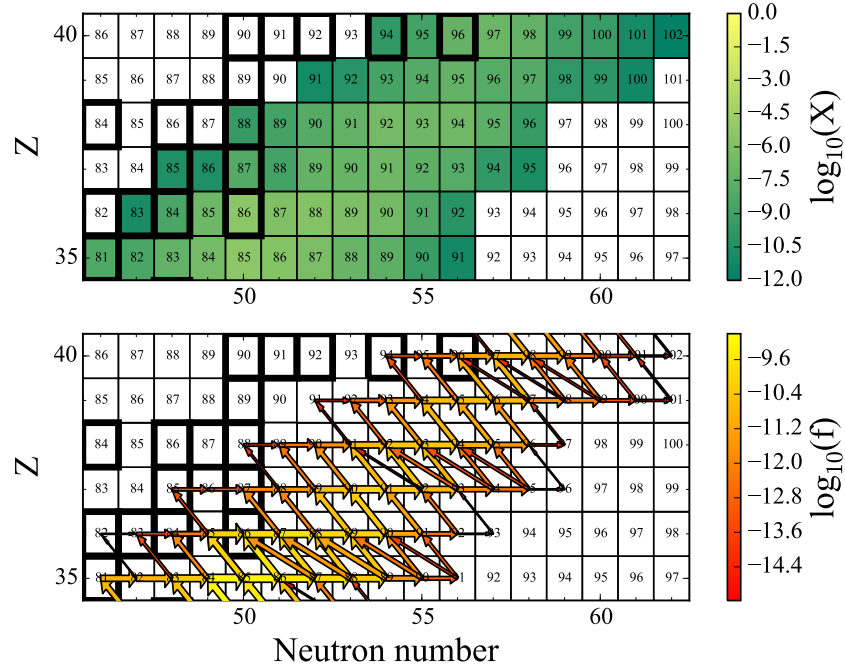


Figure 2. The mass fractions (upper panel) and reaction fluxes (lower panel) in the region of the chart of nuclides that surrounds the Rb, Sr, Y and Zr isotopes, shown for the 518th cycle of our benchmark one-zone simulation of the i process. At this cycle, the model has $\log_{10} N_n = 15.72$ and $\tau = 0.26 \text{ mbarn}^{-1}$. The nucleosynthesis flux, $f = (\delta Y_i / \delta t)_j$, shows the variation rate of the abundance $Y_i = X_i / A_i$ due to the reaction j . The arrow width and color correspond to the flux strength. Heavy-lined boxes show the stable isotopes. Most of the unstable isotopes connected by the horizontal arrows (n -capture reactions) in the lower panel have been selected for our (n,γ) reaction rate uncertainty analysis in figure 8.

of stability (figure 2). While the beta-decay rates are experimentally known (though corrections for the stellar environment may be necessary), the neutron capture rates have to be predicted using the appropriate theory to calculate neutron capture cross sections with the Hauser-Feshbach model of statistical decay of a compound nucleus. This theoretical model describes the decay of “highly” excited nuclei with large numbers of levels per MeV, provided that a reasonable description of nuclear statistical properties (for example level density and gamma ray strength function) and nuclear potentials are available. While experimental information does exist for stable nuclei, away from stability these properties have to be calculated by theoretical models. Because these models are not significantly constrained experimentally so far away from stability, various combinations of models can be used to provide equally convincing descriptions of the nuclear statistical properties. In a preliminary study, Bertolli et al. (2013) have investigated how those uncertainties propagate to calculations of observable element ratios in i -process models ($[\text{Ba}/\text{La}]$ and $[\text{La}/\text{Eu}]$ ratios). Two types of uncertainty were considered: statistically correlated uncertainties within a given model combination and a systematic type of uncertainty from the choice of particular model combinations to

describe the statistical properties of the nucleus. The uncertainties of the first type reflect the precision in reproducing model parameters known empirically from systematic studies within the valley of stability, while the second type of uncertainty is related to the accuracy of any given model combination in describing the nuclear statistical properties. They found that the dominant source of uncertainty is the systematic uncertainty that is related to the modelling choices for the nuclear statistical properties. The resulting variations of [Ba/La] and [La/Eu] ratios were so significant that the authors concluded that nuclear physics uncertainties strongly limit, at present, the predictive power of i -process simulations and that it would be very important to further study the impact of nuclear physics uncertainties on the i -process element production at various sites.

We have identified a subset of isotopes whose (n,γ) cross sections may affect the final abundances of Rb, Sr, Y and Zr in the i process. These are the 52 unstable isotopes connected by horizontal arrows in the bottom panel of figure 2. They are highlighted with the blue, green, orange and red colors in figure 3.

In i -process conditions, each isotope in the entire considered region of unstable species through which the reaction flux passes acts as a branching point. The observed elemental abundance ratios under investigation here are particularly sensitive to these branching points as each elemental abundance (except for Zr) is dominated by only one stable isotope that is fed by all isotopes on the neutron-rich isobar. Therefore, each branching point, and thus each isotopic cross section may directly affect the elemental abundance prediction that can be compared to the observed elemental abundance.

To study the effect of nuclear physics uncertainties to the corresponding reaction rates and finally to the abundances of elements from Rb to Zr, we probed the above mentioned systematic uncertainty by performing sets of suitable Hauser-Feshbach calculations of the (n,γ) reaction rates of interest at a temperature of 2×10^8 K. Our calculations are based on a set of Hauser-Feshbach models that reproduce experimentally known reaction rates close to the region of interest typically within a factor of 3. A detailed description of the models used is given in table 1. Out of the six nuclear level density (NLD) models available in TALYS§, the temperature-dependent Hartree Fock-Bogolyubov level densities using the Gogny force based on Hilaire’s combinatorial tables (Hilaire et al., 2012) were found during test calculations to produce unphysically strong odd-even effects on the neutron capture reaction rates away from stability. This could be related to systematic disagreements with experimental data mentioned by Hilaire et al. (2012) for odd-odd and odd-A nuclei. Furthermore, this model is often not able to reproduce the almost exponential behavior observed experimentally for the level density (Hilaire et al., 2012; Voinov et al., 2009; Guttormsen et al., 2013). This possibly unphysical behaviors warrant further investigation and hence the corresponding level density model was deemed not suitable for the sensitivity study of this work. Out of the five available γ ray strength function (γ SF) parametrizations, the Brink-Axel single Lorentzian formula (Brink, 1957; Axel, 1962) is known to exhibit a cut-off at

§ URL: <http://talys.eu>

Table 1. List of models used to describe the NLD and γ SF in the Hauser-Feshbach calculations of figure 3.

Nuclear Level Density (NLD) models
Constant Temperature matched to the Fermi Gas (CT+BSFG) (Dilg et al., 1973)
Back-shifted Fermi Gas (BSFG) (Dilg et al., 1973; Gilbert and Cameron, 1965)
Generalized Super fluid (GSM) (Ignatyuk et al., 1979; Ignatyuk et al., 1993)
Hartree Fock using Skyrme force (HFS) (Goriely et al., 2001)
Hartree-Fock-Bogoliubov + combinatorial (HFBS-C) (Goriely et al., 2008)
Combinations of NLD and γ ray Strength Function (γ SF) models used in the paper
CT+BSFG with Kopecky-Uhl generalized Lorentzian (KU) (Kopecky and Uhl, 1990)
BSFG with Hartree-Fock BCS + QRPA (HF-BCS+QRPA) (Capote et al., 2009)
GSM with Hartree-Fock-Bogolyubovi + QRPA (HFB+QRPA) (Capote et al., 2009)
HFS with Modified Lorentzian (Gor-ML) (Goriely, 1998)

lower γ ray energies at the limit of $E_\gamma \rightarrow 0$ that has been shown not to agree with experimental data for neutron capture reactions (Kopecky and Uhl, 1990). In general, this model is known to consistently overestimate average and total radiative widths as well as experimental neutron-capture cross sections for stable nuclei (Kopecky and Uhl, 1990; Capote et al., 2009). Therefore it was also not used in this work.

In the calculations, the NLD and γ SF models were varied systematically (see table 1 for details on the models used) within the code. All combinations of the five models of table 1 calculating the NLD with the four models to reproduce the γ SF were used. The ratio between the largest and smallest neutron capture rate is plotted in figure 3 overlaid on a segment of the table of isotopes. The maximum and minimum values of this ratio for each reaction we consider to be indicative only of the systematic uncertainty of the theoretical reaction rates without being an exhaustive way to calculate the uncertainty. The aim of the calculations was to illustrate sensitivity to the choice of theoretical model description rather than to estimate the statistical uncertainty propagated through the choice of parameter values. Relevant studies (such as the one by Bertolli et al. (2013) discussed above) suggest that this "statistical" uncertainty is small in comparison, and typically up to a factor of the order of 2. Hence, no variation of individual model parameters was attempted. It has to be noted that calculations with the Koning-Delaroche (Koning and Delaroche, 2003) optical potential and the Jeukenne-Lejonne-Mahaux (Jeukenne et al., 1977) Nuclear Matter approach were performed and yielded no significant differences to the reaction rate for the nuclei studied here. For the sake of simplicity therefore, the Koning-Delaroche potential was adopted throughout the calculations of figure 3.

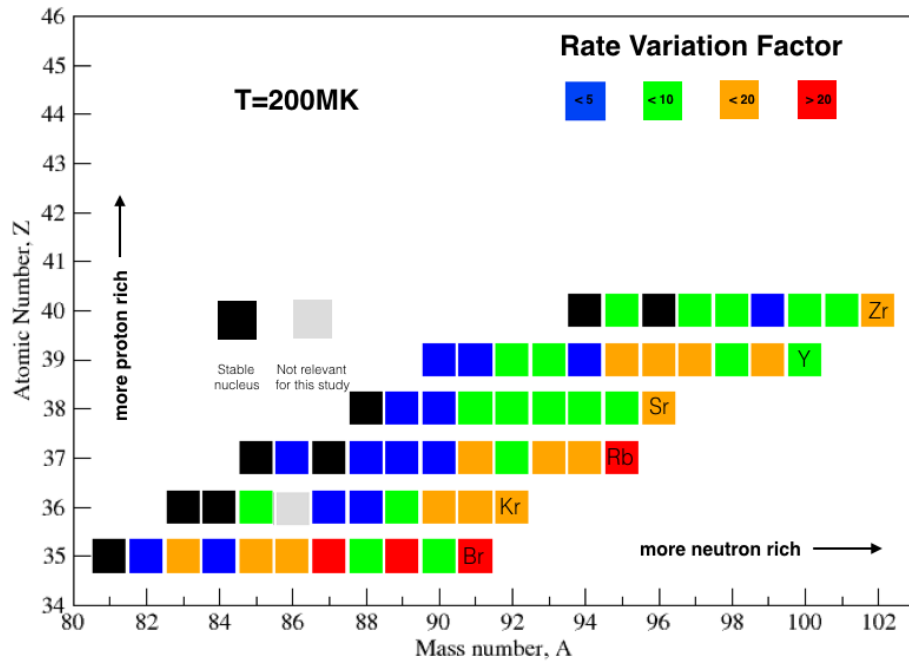


Figure 3. A mapping of the total variation factor found for each of the 52 unstable isotopes considered in this study. The ratio of maximum/minimum rate is plotted overlaid on a segment of the table of isotopes.

3. Methods and models used in our simulations of the i process

We have performed both one-zone and multi-zone simulations to model the observed abundance distribution in Sakurai’s object. At the end of this section we describe models of i process in rapidly accreting white dwarfs that require the same nuclear data of n -rich unstable species near the first peak.

3.1. Multi-zone simulations

For the multi-zone simulations of the i process in Sakurai’s object, we use the NuGrid model `mppnp_hif`. The NuGrid collaboration has for its single- and multi-zone codes a library of examples that represent a wide range of nuclear astrophysics conditions for nucleosynthesis. The `mppnp_hif` model is one of these examples and represents the scenario described in Herwig et al. (2011). The name `mppnp_hif` means the multi-zone post-processing nucleosynthesis parallel code (Pignatari et al., 2016) customized for the problem of hydrogen ingestion flash. The simulations take temperature, density and diffusion coefficient profiles for the He convective zone in the mass range $0.57556 \leq M_r/M_\odot \leq 0.5987$ from the stellar evolution model ET14 of an asymptotic giant branch star of Herwig et al. (2006) during its last thermal pulse. This model

(“RUN48/strat-B” in figure 9 of Herwig et al. (2011)) reproduces the observed ratio of the total abundances of selected elements from the second and first s-process peaks in Sakurai’s object if *ad-hoc* mixing assumptions beyond the mixing-length theory are made. The ingestion of H into the He-shell convection zone is taken into account in a parameterized way, by adding $\Delta X = 5 \times 10^{-4}$ of H to the upper $4 \times 10^{-4} M_{\odot}$ of the He convective zone at nearly every 6th minute, which corresponds to the H entrainment rate of $5.3 \times 10^{-10} M_{\odot} \text{ s}^{-1}$. The split of the zone is assumed to occur after nearly 1000 minutes. More details on the multi-zone simulation setup can be found in section 5.1 of Herwig et al. (2011). Note that the benchmark multi-zone simulations for the present analysis are all done with their RUN48 model. Herwig et al. (2011) also considered other models, with different elemental ratios obtained in the Rb-Zr mass region. However, the conclusions of this work are not expected to change if these other models are used.

The initial abundances are taken from the Solar System abundance distribution of Asplund et al. (2005) with isotopic ratios from Lodders (2003) scaled to the heavy-element mass fraction $Z = 0.01$. The initial abundances $X(^4\text{He}) = 0.35$, $X(^{12}\text{C}) = 0.43$, and $X(^{16}\text{O}) = 0.19$ (Herwig et al., 1999) reflect the primary production of ^{12}C and ^{16}O in the He shell. In the multi-zone case, the initial abundances of a number of isotopes participating in the pp chains, CNO cycle and He burning are also modified to take into account their changes during the evolution of the star prior to its VLTP, as calculated by Herwig et al. (1999).

The benchmark multi-zone post-processing nucleosynthesis simulations of the i process in Sakurai’s object were run with dynamically updated, based on the strength of the nucleosynthesis fluxes, lists of ~ 5300 isotopes and ~ 67000 nuclear reactions. Most reaction rates were taken from the JINA REACLIB v1.1 library (Cyburt et al., 2010) with the following exceptions. The NACRE recommended rates (Angulo et al., 1999) were used for all of the CNO cycle reactions, except $^{13}\text{N}(p,\gamma)^{14}\text{O}$ and $^{14}\text{N}(p,\gamma)^{15}\text{O}$ for which the JINA REACLIB rates were used. The rates of the proton-induced reactions for isotopes with $A = 20-40$ were taken from Iliadis et al. (2001). For the (n,γ) reactions with isotopes located along the valley of stability, we mainly used the revision 0.3 of KADoNIS data^{||} (Dillmann et al., 2006). The compilations of Fuller et al. (1985), Oda et al. (1994), and Goriely (1999) provide the NuGrid codes with weak reaction rates. To speed up our multi-zone simulations for the uncertainty study that requires a large number of runs, we have cut off the network at Ag, which reduced the number of isotopes to ~ 400 . We have checked that this does not change the final distribution of elements lighter than Ag and, in particular, the final abundances of Rb, Sr, Y and Zr, as compared to the benchmark case.

3.2. One-zone simulations

For the one-zone simulations of the i process in Sakurai’s object, we use the same NuGrid model as in Dardelet et al. (2014). The one-zone simulation setup assumes

^{||} **URL:** <http://www.kadonis.org>

constant temperature and density, for which we adopt the typical He-shell condition values of $T = 2 \times 10^8$ K and $\rho = 10^4$ g cm $^{-3}$ and is evolved using the NuGrid single-zone nucleosynthesis code PPN.

Similar to the multi-zone case, the initial abundances for the one-zone simulations are taken from the Solar System abundance distribution of Asplund et al. (2005) with isotopic ratios from Lodders (2003) scaled to the heavy-element mass fraction $Z = 0.01$. In the one-zone model, we adopt $X(^1\text{H}) = 0.1$, which is supposed to mimic the H ingestion into the He convective zone, and $X(^{12}\text{C}) = 0.5$ at the expense of ^{16}O . This H abundance is much higher than that expected in any zone of more realistic 1D or 3D multi-zone simulations. However, this initial condition in the one-zone model reproduces neutron densities of the i process (Dardelet et al., 2014).

All of our one-zone post-processing nucleosynthesis simulations of the i process in Sakurai’s object were run with the same lists of isotopes and nuclear reactions and used the same reaction rates as our benchmark multi-zone simulations.

3.3. NuSensi

The one-zone computations of i -process nucleosynthesis are much faster than their multi-zone counterparts. Therefore, whenever possible one may use these for reaction rate sensitivity studies involving multiple simulation runs. The NuSensi framework provides utilities to perform such a study based on large sets of one-zone simulations with specified modifications to reaction rates for selected isotopes. The tools allow to post-process thermodynamic trajectories from NuGrid’s suite of examples, such as the i -process example (Dardelet et al., 2014). Various trajectories derived from AGB models, massive star models and core-collapse supernova explosion models are available in the example suite.

To test the impact of reaction rates on the production of species, a set of simulations corresponding to a list of user-defined reactions and their rate multiplication factors f_j are performed in parallel. A default reaction rate r_j^0 is modified to a new rate $r_j^1 = f_j r_j^0$. The list of reactions and multiplication factors can be provided by hand or via a selection menu. It can also be generated automatically for a specific area of the network. Multiple reaction rates can be changed with different f factors for a single simulation, except when a network area is adopted and the same f factor is applied to all rates.

The results are then analyzed primarily via a matrix of sensitivity factors

$$S_{i,j} = \frac{\Delta X_i / X_i}{\Delta r_j / r_j} = \frac{\Delta X_i / X_i}{f_j - 1}, \quad (1)$$

where ΔX_i is the abundance change for the i -th isotope and Δr_j is the change of the reaction rate r_j (Koloczek et al., 2016). The columns and rows of the sensitivity matrix correspond, respectively, to the reactions and species included in the sensitivity study. Sensitivity factors based on decayed and undecayed abundances can be calculated.

The sensitivity factors are best visualised via an isotopic abundance chart as shown in figure 4 for the sensitivity study of abundances of stable isotopes to the $^{89}\text{Kr}(n,\gamma)^{90}\text{Kr}$

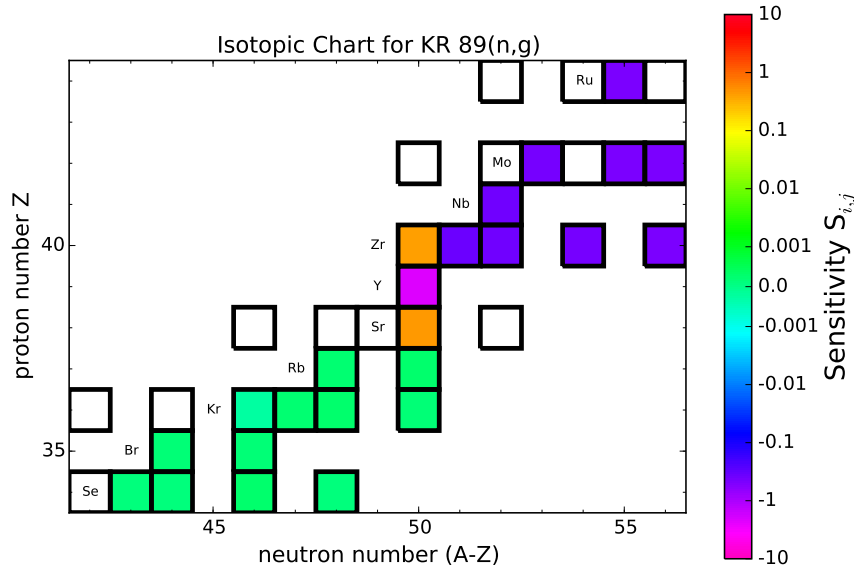


Figure 4. The isotopic chart with sensitivity factors based on the $^{89}\text{Kr}(n,\gamma)^{90}\text{Kr}$ reaction rate changed by the factor $f = 0.1$.

reaction rate based on its change by the factor $f = 0.1$ (as suggested by figure 3).

3.4. Rapidly accreting white dwarfs (RAWDs)

When a carbon-oxygen white dwarf is a primary component of a close binary system with a main-sequence or subgiant star as a secondary component, it can accrete H-rich material from its companion at a sufficiently high rate of $\sim 10^{-7} M_{\odot} \text{ yr}^{-1}$ that guarantees stationary H burning at its surface. As a result, a He shell surrounded by a thin H envelope is accumulated on such a rapidly accreting white dwarf (RAWD). When its mass reaches a certain limit ($\sim 0.01 - 0.03 M_{\odot}$), the He shell will experience a thermal flash, and the following evolution of the RAWD, including H ingestion by the He-shell convection and ensuing nucleosynthesis, should thereafter be very similar to that of Sakurai's object, except that RAWDs can experience tens of He-shell flashes and, therefore, be important polluters of interstellar medium with the products of i -process nucleosynthesis. Here, we use the RAWD model A of Denissenkov et al. (2016). It has at least two episodes of H ingestion by the He-shell convection driven by the same thermal pulse, the one being H ingestion on the timescale of 0.38 yr that is immediately followed by the other episode of H ingestion on the timescale of 0.0084 yr. These are the results obtained with a one-dimensional stellar evolution code. Unfortunately, without 3D hydrodynamic simulations of the process of H ingestion in RAWDs, results of which can be very surprising, as demonstrated by Herwig et al. (2014), we cannot decide which of the two episodes (or maybe both of them) better describes the H ingestion in a real

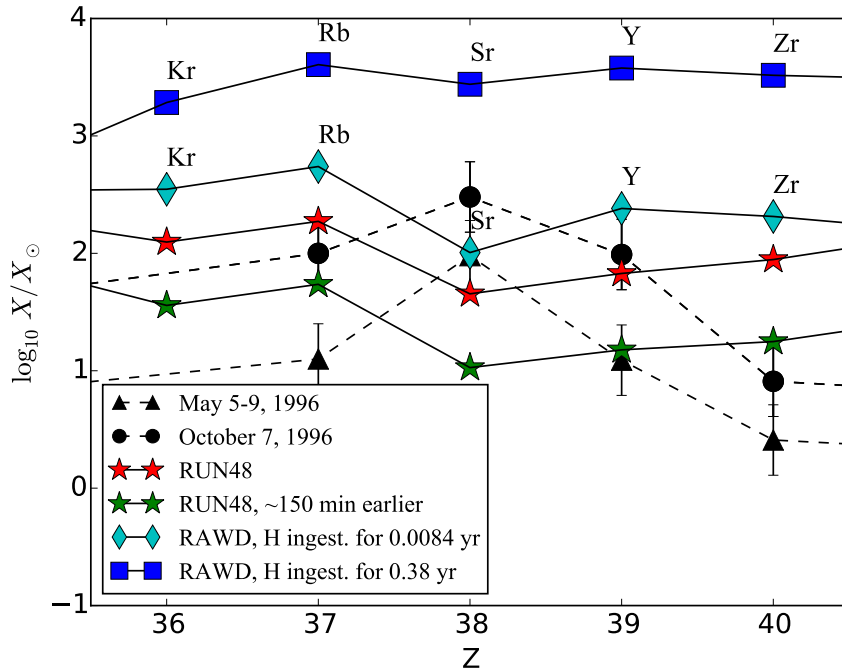


Figure 5. A comparison of the final abundances of Rb, Sr, Y and Zr predicted (symbols in color) for the i -process nucleosynthesis models of Sakurai’s object (RUN48) and for a model of a rapidly-accreting white dwarf (RAWD) with the abundances of these elements measured in Sakurai’s object at two different epochs (black symbols) by Asplund et al. (1999). The simulation results for the RAWD model are shown for two cases of H ingestion on the timescales 0.0084 yr and 0.38 yr (see text). All unstable isotopes, including the long-lived ^{90}Sr , were assumed to have decayed.

RAWD. For the both H-ingestion episodes, the ensuing nucleosynthesis is simulated using the `mppnp_hif` example with parameters taken from the RAWD model A.

4. Results

4.1. Multi-zone simulations

In figure 5, we compare predicted abundances of Rb, Sr, Y and Zr with those measured by Asplund et al. (1999) in Sakurai’s object on the 5th to 9th May and five months later, on the 7th of October of the year 1996. The red star symbols represent the final abundances from our benchmark multi-zone model, as in figure 1, while the green star symbols are abundances from the same model, but taken at ~ 150 minutes earlier. As explained earlier, the time of the observations is a few years after the time when the i process occurs close to the peak of the He-shell flash that drives the H ingestion. The abundance patterns observed at different times are very similar, and the model abundance patterns are also similar to each other. None of these variations explains the difference between observations and models.

The dark blue squares and the light blue diamonds in figure 5 represent the final

abundances at the surface of the He convective zone of the RAWD model A for the two episodes of H ingestion that lasted 0.38 yr and 0.0084 yr.

All of the four predicted abundance profiles in figure 5 look, on the one hand, similar to each other, but, on the other hand, differently from the two observed abundance profiles. Nuclear physics uncertainties alone can not account for the difference between model predictions and observations, and stellar model parameters and assumptions need to be analyzed for their complete error budget.

Qualitatively, the difference between the predicted and observed profiles is manifested by the sign and/or magnitude of the abundance change when we go along the profiles from Rb to Sr, then from Sr to Y and, finally, from Y to Zr. The first of these findings has motivated us to carry out a sensitivity and uncertainty study of nuclear reactions relevant to changes of abundances of Rb, Sr, Y and Zr at i -process conditions, namely of the (n,γ) cross sections of the 52 unstable isotopes from figure 3. The second has prompted us to use $([Rb/Sr],[Y/Sr])$ and $([Sr/Y],[Zr/Y])$ planes in our analysis, because it is relationships between abundance ratios of neighbouring elements that determine a shape of abundance profile.

The results of the nucleosynthesis calculations presented in figure 5 are obtained assuming that all unstable isotopes have decayed instantaneously at the end of simulations. This is a good assumption for most of the considered isotopes, that have relatively short half-life times, except ^{90}Sr , whose half-life of 28.9 yr is longer than the duration of the H-ingestion convective He-shell flash in Sakurai's object followed by the expansion and approach of the star to the AGB (~ 2 yr Herwig (2001*b*)). This affects the predicted abundance of Zr, because the final abundance of ^{90}Sr , before it decays into ^{90}Zr , is comparable with the final abundance of ^{96}Zr that becomes the most abundant Zr isotope in our simulations. If we do not allow ^{90}Sr to decay then its final abundance has to be subtracted from the final abundance of Zr. When we do this for the benchmark multi-zone case, the final Zr abundance is reduced by 0.25 dex. This estimate is obtained using the final mass-averaged abundances at the top of the He convective zone, where the mass fraction of the stable isotope ^{88}Sr exceeds the mass fraction of the unstable ^{90}Sr , therefore the assumption about the complete decay of ^{90}Sr does not affect the total abundance of Sr. In our reaction rates sensitivity study, results of which are presented in the next section, we explicitly assume that ^{90}Sr has not at all decayed.

4.2. Uncertainty study based on one-zone simulations

Before our reaction rate sensitivity study with NuSensi, we have to find a timestep (cycle) of the benchmark one-zone simulations of the i -process nucleosynthesis at which the abundances of Rb, Sr, Y and Zr have approached as close as possible their final values obtained in the benchmark multi-zone case. Such a calibration of the one-zone simulation setup by the multi-zone simulation results is needed because the abundance distribution emerging in the one-zone simulations changes with time much faster than in the multi-zone simulations due to the fact that the former essentially replace the entire

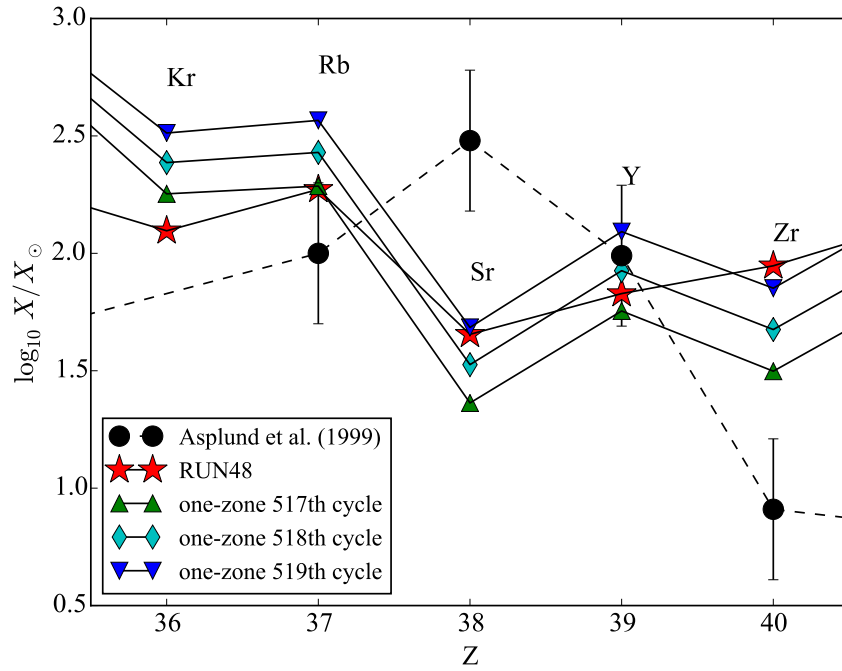


Figure 6. At the 518th timestep (cycle) of the benchmark one-zone simulations, the Rb, Sr, Y and Zr abundance distribution (diamonds) approaches as close as possible its corresponding final abundance distribution from the benchmark multi-zone simulations (stars) of the i process in Sakurai's object. It is this PPN cycle number that should be used in the one-zone reaction rate uncertainty study to reach conclusions similar to those expected from the corresponding multi-zone simulations.

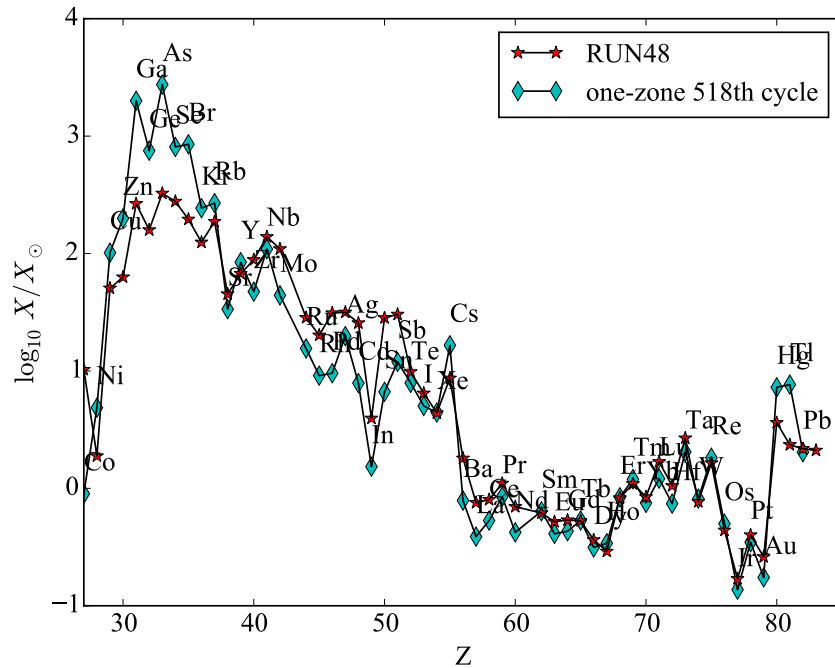


Figure 7. Similar to figure 6, but for a larger number of the elements heavier than Co.

He convective zone by a single zone that cannot replenish seeds for neutron capture by mixing. A comparison of the final abundances of Rb, Sr, Y and Zr from the multi-zone model with the abundances of these elements from the one-zone simulations shows that their distributions become as close as possible to each other at the 518th cycle (figure 6). Figure 7, in which a similar comparison is made for a much larger number of the elements heavier than Co, shows that if we chose a different set of neighbouring elements for a reaction rate sensitivity study then we would have to adopt a different cycle from one-zone simulations as a representative one for a comparison with final abundances from the multi-zone case. For instance, at the Zn-As region we would need an earlier (the 507th) timestep than the 518th. This is because the interplay between the total amount of neutrons made and the dynamic variation of iron seeds in the full model, cannot be reproduced by one-zone simulations for the complete neutron-capture path between Fe and Bi.

In our reaction rate sensitivity study, we have used the 518th cycle as the end point of one-zone simulations of the i -process nucleosynthesis. We ran 104 one-zone simulations, in which the (n,γ) cross sections of the 52 unstable isotopes from figure 3 were varied up and down by their respective total variation factors that were estimated from the nuclear physics uncertainties and color-coded in that map (for the estimate shown as > 20 , we have used a factor of 30). The resulting changes in the final abundance ratios are shown in figure 8, assuming that ^{90}Sr has not decayed. The numbers in the panels correspond to the sequential positions of the considered reactions in a log file generated by a NuSensi shell script. The large zero symbol represents the benchmark one-zone results. The largest deviations from the benchmark results in both upper and down variation cases are obtained for the numbers 4, 18 and 35 which correspond to ^{88}Kr , ^{89}Kr and ^{85}Br , therefore these isotopes should be considered as the first candidates for a follow-up experimental measurement of their (n,γ) cross sections.

Although the one-zone simulations are able to catch the most outstanding isotopes, whose reaction rate uncertainties will have the strongest impact on the predicted nucleosynthesis yields, they may miss some more subtle cases that can only be revealed in multi-zone sensitivity studies. As an example, figure 9 shows that our one-zone simulations have missed a potentially important case of ^{89}Rb . When its (n,γ) cross section is reduced by a factor of 5 simultaneously with that of ^{88}Kr , which is within the nuclear physics uncertainties (figure 3), we get the final abundances of Sr and Zr closer to their observed values, while the final abundances of Rb and Y remain, respectively, the same and within the observational errors. A comparison of panels A and B in figure 9 shows that the failure of the one-zone simulations to catch the ^{89}Rb case is caused by the fact that their benchmark Y abundance is higher than the benchmark multi-zone Y abundance and that the only effect from the reduction of the ^{89}Rb n-capture rate is the increase of the Y abundance. The reduction of the ^{88}Kr n-capture rate, on the other hand, leads to the shift of the Sr and Zr abundances in the direction of their observed values, while the Y abundance moves away from its observed value. When the two reaction rates are reduced simultaneously, we get the final predicted abundances in

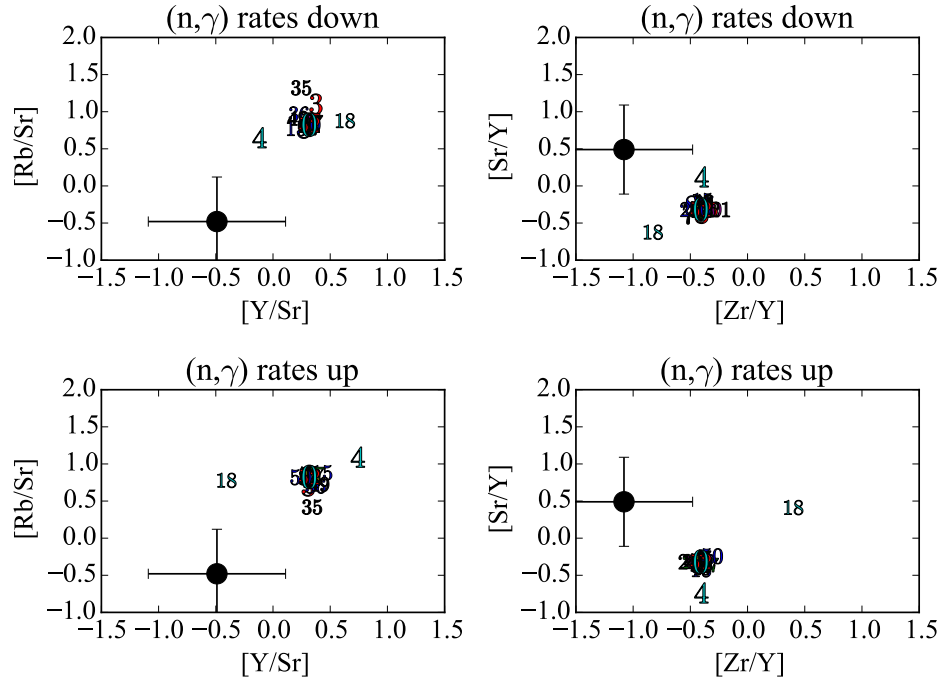


Figure 8. The changes of the Rb, Sr, Y and Zr abundance ratios produced by the variations (up and down) of the n -capture cross sections applied individually to each of the 52 unstable isotopes highlighted with the blue, green, orange and red colors in figure 3. The ^{90}Sr isotope was not allowed to decay in these calculations. The maximum variation factors corresponding to the colors (a factor of 30 for the red color) have been used in these one-zone computations. The numbers in the panels give the sequential positions of the (n,γ) reactions in the NuSensi log file. For comparison, the abundance ratios predicted for the benchmark one-zone case and those measured in Sakurai’s object by Asplund et al. (1999) are shown with the zero symbol and filled circle with errorbars. The outstanding cases 4, 18 and 35 that correspond to the isotopes ^{88}Kr , ^{89}Kr and ^{85}Br deserve experimental measurements of their (n,γ) rates.

a better agreement with the observed ones. This example demonstrates that reaction rate sensitivity studies based on one-zone simulations should be complemented with multi-zone simulations, the latter being applied to individual reaction rates when there is a suspicion that some potentially important cases have been missed in the survey one-zone simulations.

5. Summary and Conclusions

We have used the NuGrid framework and its NuSensi tool in our reaction rate sensitivity study of the i -process nucleosynthesis model of the post-AGB star Sakurai’s object. The 52 unstable isotopes of Br, Kr, Rb, Sr, Y and Zr (the color squares in figure 3) relevant to the i -process production of Rb, Sr, Y and Zr, whose abundances were measured in the atmosphere of Sakurai’s object by Asplund et al. (1999), have been selected for this study. The (n,γ) cross sections of the selected isotopes have the

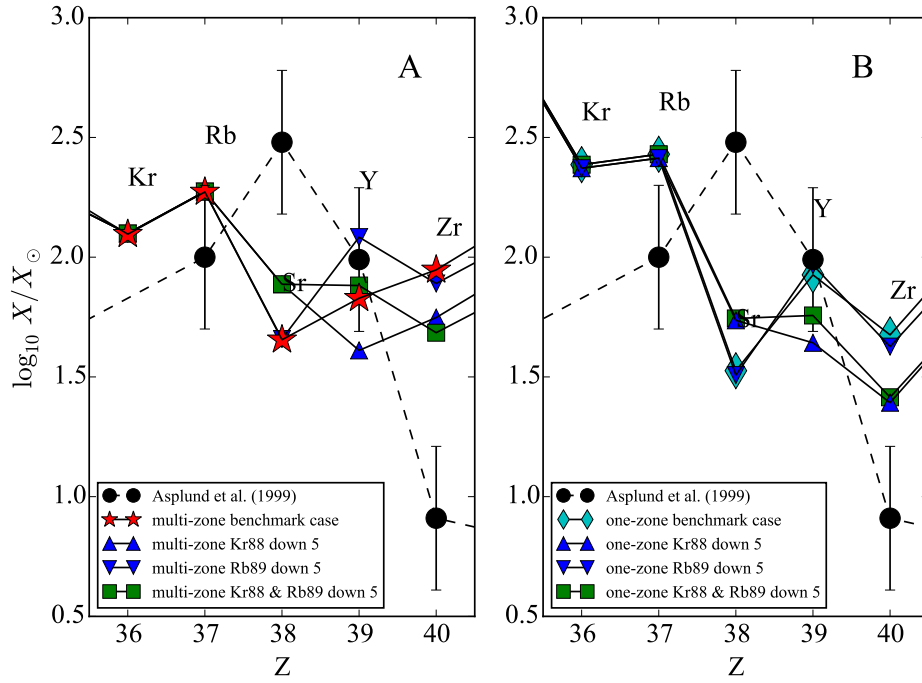


Figure 9. The results of the reaction rate sensitivity studies for the ^{88}Kr and ^{89}Rb isotopes in the multi-zone (panel A) and one-zone (panel B) cases. In both panels, the benchmark model predictions are compared with the results obtained when the (n,γ) cross sections of these isotopes have been reduced by a factor of 5 individually (the blue up and down triangles) and simultaneously (the green squares).

nuclear physics uncertainties (color-coded in figure 3) ranging from a factor of < 5 to more than 20, as estimated in the present work. We have varied the n-capture rates up and down, applying the mapped uncertainty variation factors individually to each of the 52 isotopes per one simulation run, thus carrying out 104 runs in total. One-zone post-processing nucleosynthesis simulations are much faster than their multi-zone counterparts. However, they have to be calibrated, using the final results of their corresponding multi-zone simulations, to find a timestep (cycle) at which the distribution of abundances of the elements included in the study obtained in the one-zone simulations resembles as much as possible the final abundance distribution of these elements in the multi-zone simulations. In our case, we have found that the benchmark one-zone simulations terminated at the 518th cycle produce the relative distribution of the Rb, Sr, Y and Zr element abundances closest to the final one from the benchmark multi-zone case (figure 6). The results of our n-capture reaction rate sensitivity study have been plotted on the $([\text{Rb}/\text{Sr}], [\text{Y}/\text{Sr}])$ and $([\text{Sr}/\text{Y}], [\text{Zr}/\text{Y}])$ planes (figure 8), because relationships between these abundance ratios determine the shape of the element abundance distribution in the Rb-Zr region, which is different for the predicted and observed abundances (figure 5). Our analysis has shown that the estimated uncertainties of the (n,γ) cross sections of ^{88}Kr , ^{89}Kr and ^{85}Br have the strongest effect on the predicted abundance ratios, therefore they have a high priority to

be the target for future experimental campaigns. We have also found that, because of its simplified nature compared to the multi-zone simulation setup, the one-zone simulations have missed a potentially important case of ^{89}Rb . When its n -capture rate is reduced by the factor of 5 simultaneously with the similar variation of the ^{88}Kr n -capture rate, this improves the agreement between the predicted and observed abundances of Rb, Sr, Y and Zr in Sakurai’s object. This means that, although being fast, the one-zone simulations used for reaction rate sensitivity studies should be complemented with selected multi-zone simulations to analyze sensitivities of predicted nucleosynthesis yields to uncertainties of some individual reaction rates whose potentially important impact on final results is suspected to have been overlooked in the one-zone simulations. In cases, such as the white dwarf He-shell flash H-ingestion i process, where three-dimensional hydrodynamic effects will be important, we cannot entirely exclude that further (n,γ) reactions could be identified as important for such more realistic models. Unfortunately the computational tools for such three-dimensional i -process models are not yet available.

In this work we have shown that the nuclear physics data uncertainties contribute significantly to the total error budget of i -process model predictions. However, nuclear physics data improvements will not alone close the gap between model predictions and observations for Sakurai’s object. This implies that, in addition to improve the nuclear data, further efforts have to be made to improve the stellar models. Especially, the 3D hydrodynamic effects in convective-reactive H-ingestion flashes (Herwig et al., 2014) may play an important role.

Acknowledgments

This material is based upon work supported by the National Science Foundation under Grant No. PHY-1430152 (JINA Center for the Evolution of the Elements). M. P. acknowledges the support from the “Lendület-2014” Programme of the Hungarian Academy of Sciences and from SNF (Switzerland). F. H. receives NSERC funding through a Discovery grant. S. J. is a fellow of the Alexander von Humboldt Foundation and acknowledges support from the Klaus Tschira Stiftung.

References

- Angulo C, Arnould M, Rayet M, Descouvemont P, Baye D, Leclercq-Willain C, Coc A, Barhoumi S, Aguer P, Rolfs C, Kunz R, Hammer J W, Mayer A, Paradellis T, Kossionides S, Chronidou C, Spyrou K, degl’Innocenti S, Fiorentini G, Ricci B, Zavatarelli S, Providencia C, Wolters H, Soares J, Grama C, Rahighi J, Shotton A and Laméhi Rachti M 1999 *Nuclear Physics A* **656**, 3–183.
- Asplund M, Grevesse N and Sauval A J 2005 in T. G Barnes, III and F. N Bash, eds, ‘Cosmic Abundances as Records of Stellar Evolution and Nucleosynthesis’ Vol. 336 of *Astronomical Society of the Pacific Conference Series* p. 25.
- Asplund M, Lambert D L, Kipper T, Pollacco D and Shetrone M D 1999 *A&A* **343**, 507–518.
- Axel P 1962 *Physical Review* **126**, 671–683.

- Beers T C and Christlieb N 2005 *Annu. Rev. Astro. Astrophys.* **43**(1), 531–580.
- Bertolli M G, Herwig F, Pignatari M and Kawano T 2013 *arXiv:1310.4578 [astro-ph.SR]*.
- Bisterzo S, Gallino R, Straniero O, Cristallo S and Käppeler F 2012 *MNRAS* **422**, 849–884.
- Brink D M 1957 *Nucl. Phys. A* **4**, 215–220.
- Campbell S W, Lugaro M and Karakas A I 2010 *A&A* **522**, L6.
- Capote R, Herman M, Obložinský P, Young P, Goriely S, Belgia T, Ignatyuk A, Koning A, Hilaire S, Plujko V, Avrigeanu M, Bersillon O, Chadwick M, Fukahori T, Ge Z, Han Y, Kailas S, Kopecky J, Maslov V, Reffo G, Sin M, Soukhovitskii E and Talou P 2009 *Nuclear Data Sheets* **110**(12), 3107 – 3214. Special Issue on Nuclear Reaction Data.
URL: <http://www.sciencedirect.com/science/article/pii/S0090375209000994>
- Cowan J J and Rose W K 1977 *ApJ* **212**, 149–158.
- Cyburt R H, Amthor A M, Ferguson R, Meisel Z, Smith K, Warren S, Heger A, Hoffman R D, Rauscher T, Sakharuk A, Schatz H, Thielemann F K and Wiescher M 2010 *ApJS* **189**, 240–252.
- Dardelet L, Ritter C, Prado P, Heringer E, Higgs C, Sandalski S, Jones S, Denisenkov P, Venn K, Bertolli M, Pignatari M, Woodward P and Herwig F 2014 in ‘Proceedings of XIII Nuclei in the Cosmos (NIC XIII). 7-11 July, 2014. Debrecen, Hungary. Online at <http://pos.sissa.it/cgi-bin/reader/conf.cgi?confid=204>’ p. 145.
- Denissenkov P, Herwig F, Battino U, Ritter C, Pignatari M, Jones S and Paxton B 2016 *arXiv:1610.08541 [astro-ph.SR]*.
- Dilg W, Schantl W, Vonach H and Uhl M 1973 *Nuclear Physics A* **217**(2), 269 – 298.
URL: <http://www.sciencedirect.com/science/article/pii/0375947473901966>
- Dillmann I, Heil M, Käppeler F, Plag R, Rauscher T and Thielemann F K 2006 in A Woehr and A Aprahamian, eds, ‘Capture Gamma-Ray Spectroscopy and Related Topics’ Vol. 819 of *American Institute of Physics Conference Series* pp. 123–127.
- Fujimoto M Y, Ikeda Y and Iben Jr I 2000 *ApJ* **529**(1), L25–L28.
- Fujiya W, Hoppe P, Zinner E, Pignatari M and Herwig F 2013 *ApJ* **776**, L29.
- Fuller G M, Fowler W A and Newman M J 1985 *ApJ* **293**, 1–16.
- Gilbert A and Cameron A G W 1965 *Canadian Journal of Physics* **43**(8), 1446–1496.
URL: <http://dx.doi.org/10.1139/p65-139>
- Goriely S 1998 *Physics Letters B* **436**(1–2), 10 – 18.
URL: <http://www.sciencedirect.com/science/article/pii/S0370269398009071>
- Goriely S 1999 *A&A* **342**, 881–891.
- Goriely S, Hilaire S and Koning A J 2008 *Phys. Rev. C* **78**, 064307.
URL: <http://link.aps.org/doi/10.1103/PhysRevC.78.064307>
- Goriely S, Tondeur F and Pearson J 2001 *Atomic Data and Nuclear Data Tables* **77**(2), 311 – 381.
URL: <http://www.sciencedirect.com/science/article/pii/S0092640X0090857X>
- Guttormsen M, Jurado B, Wilson J N, Aiche M, Bernstein L A, Ducasse Q, Giacoppo F, Gorgen A, Gunsing F, Hagen T W, Larsen A C, Lebois M, Leniau B, Renstrøm T, Rose S J, Siem S, Tornyi T, Tveten G M and Wiedeking M 2013 *Phys. Rev. C* **88**(2), 024307.
- Hampel M, Stancliffe R J, Lugaro M and Meyer B S 2016 *arXiv:1608.08634 [astro-ph.SR]*. *ApJ* in press.
- Herwig F 2001a *Ap&SS* **275**, 15–26.
- Herwig F 2001b *ApJ* **554**, L71–L74.
- Herwig F 2003 *CNO in the universe* **304**, 318.
- Herwig F, Austin S M and Lattanzio J C 2006 *Phys. Rev. C* **73**(2), 025802.
- Herwig F, Blöcker T, Langer N and Driebe T 1999 *A&A* **349**, L5–L8.
- Herwig F, Pignatari M, Woodward P R, Porter D H, Rockefeller G, Fryer C L, Bennett M and Hirschi R 2011 *ApJ* **727**, 89.
- Herwig F, Woodward P R, Lin P H, Knox M and Fryer C 2014 *ApJ* **792**, L3.
- Hilaire S, Girod M, Goriely S and Koning A J 2012 *Phys. Rev. C* **86**(6), 064317.
- Ignatyuk A, Istekov K and Smirenkin G 1979 *Sov. J. Nucl. Phys.* **29**, 450.

- Ignatyuk A V, Weil J L, Raman S and Kahane S 1993 *Phys. Rev. C* **47**, 1504–1513.
URL: <http://link.aps.org/doi/10.1103/PhysRevC.47.1504>
- Iliadis C, D’Auria J M, Starrfield S, Thompson W J and Wiescher M 2001 *ApJS* **134**, 151–171.
- Iwamoto N, Kajino T, Mathews G J, Fujimoto M Y and Aoki W 2004 *ApJ* **602**(1), 377–387.
- Jadhav M, Pignatari M, Herwig F, Zinner E, Gallino R and Huss G R 2013 *ApJ* **777**, L27.
- Jeukenne J P, Lejeune A and Mahaux C 1977 *Phys. Rev. C* **15**, 10–29.
- Jones S, Ritter C, Herwig F, Fryer C, Pignatari M, Bertolli M G and Paxton B 2016 **455**(4), 3848–3863.
- Käppeler F, Gallino R, Bisterzo S and Aoki W 2011 *Reviews of Modern Physics* **83**, 157–194.
- Koloczek A, Thomas B, Glorius J, Plag R, Pignatari M, Reifarth R, Ritter C, Schmidt S and Sonnabend K 2016 *Atomic Data and Nuclear Data Tables* **108**, 1–14.
- Koning A J and Delaroche J P 2003 *Nuclear Physics A* **713**, 231–310.
- Kopecky J and Uhl M 1990 *Phys. Rev. C* **41**, 1941–1955.
URL: <http://link.aps.org/doi/10.1103/PhysRevC.41.1941>
- Liu N, Savina M R, Davis A M, Gallino R, Straniero O, Gyngard F, Pellin M J, Willingham D G, Dauphas N, Pignatari M, Bisterzo S, Cristallo S and Herwig F 2014 *ApJ* **786**, 66.
- Lodders K 2003 *ApJ* **591**, 1220–1247.
- Lugaro M, Karakas A I, Stancliffe R J and Rijs C 2012 *ApJ* **747**, 2.
- Masseron T, Johnson J A, Plez B, van Eck S, Primas F, Goriely S and Jorissen A 2010 *A&A* **509**, A93.
- Miller Bertolami M M and Althaus L G 2007 *MNRAS* **380**(2), 763–770.
- Miller Bertolami M M, Althaus L G, Serenelli A M and Panei J A 2006 *A&A* **449**, 313–326.
- Mishenina T, Pignatari M, Carraro G, Kovtyukh V, Monaco L, Korotin S, Shereta E, Yegorova I and Herwig F 2015 *MNRAS* **446**, 3651–3668.
- Oda T, Hino M, Muto K, Takahara M and Sato K 1994 *Atomic Data and Nuclear Data Tables* **56**, 231–403.
- Pignatari M, Herwig F, Hirschi R, Bennett M, Rockefeller G, Fryer C, Timmes F X, Ritter C, Heger A, Jones S, Battino U, Dotter A, Trappitsch R, Diehl S, Frischknecht U, Hungerford A, Magkotsios G, Travaglio C and Young P 2016 *The Astrophysical Journal Supplement Series* **225**.
- Roederer I U, Karakas A I, Pignatari M and Herwig F 2016 *ApJS* **821**(1), 37.
- Stancliffe R J, Dearborn D S P, Lattanzio J C, Heap S A and Campbell S W 2011 *ApJ* **742**, 121.
- Thielemann F K, Arcones A, Käppeli R, Liebendörfer M, Rauscher T, Winteler C, Fröhlich C, Dillmann I, Fischer T, Martinez-Pinedo G, Langanke K, Farouqi K, Kratz K L, Panov I and Korneev I K 2011 *Progress in Particle and Nuclear Physics* **66**, 346–353.
- Voinov A V, Oginni B M, Grimes S M, Brune C R, Guttormsen M, Larsen A C, Massey T N, Schiller A and Siem S 2009 *Phys. Rev. C* **79**(3), 031301.